COMSOL
CONFERENCE
2024 FLORENCE

Monte-Carlo Model for Radiation Transport in Solid X-Ray Targets

C. Feist[1], A. Plankensteiner[2]
1. CENUMERICS, Innsbruck, Austria.
2. PLANSEE SE, Reutte, Austria.

Abstract
Implementation of a Monte-Carlo model for radiation transport in solid X-ray targets is presented. The model describes the transport of electrons and photons and their energies in a fully quantitative fashion accounting for the relevant interactions with target atoms and the production of X-ray photons by bremsstrahlung emission as well as of excited target atoms. Considering energy deposition within the target as well as target surface photon emission allows to derive fundamental dosimetry quantities such as absorbed dose, photon fluence, and photon energy fluence and guarantees energy conservation. Results obtained for an ideal monoenergetic electron pencil beam can be transformed *a posteriori* to an arbitrary electron beam shape for an isotropic medium using convolution theorem. Application of the model implemented based on the COMSOL Particle Tracing Module is demonstrated for a tungsten target exposed to a 50 keV electron beam.
Keywords: Monte-Carlo, X-ray, target, photon, electron, radiation, transport, bremsstrahlung, fluence, dose.

Introduction
X-rays are a type of high-energy electromagnetic radiation with an energy range above the ultraviolet light. They are capable to penetrate solid substances and biological tissues and are therefore widely used for medical imaging, radiotherapy, material testing and various other applications.

In these contexts, X-rays are usually produced using high-vacuum X-ray tubes (Figure 1) where electrons thermionically emitted from a cathode (C) are accelerated towards an anode (A) by the electric field from an applied direct voltage of $10^1 \ldots 10^2$ kV.

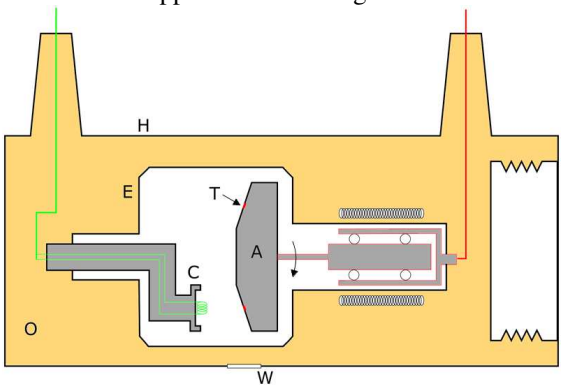

Figure 1. Schematic of typical X-ray tube (Anode, Cathode, Target, Tube Envelope, Cooling Oil, Tube Housing, Tube Window), adapted from [1].

The electrons can be focused to the required size of the focal spot on the target of the anode by electromagnetic lenses, thus, forming an electron beam. Upon their impact on the target material or focal track (T) of the anode and during subsequent penetration of the latter, electrons are decelerated through inelastic scattering by the electric field near the nuclei and emit X-ray photons. This mechanism of X-ray generation, termed as *bremsstrahlung* emission, results in a continuous energy spectrum. On the other hand, X-rays are produced by radiative transitions during relaxation of excited atoms created by inelastic electron or photon interactions with atoms. The energies of X-ray photons created by this *characteristic* emission are determined by the radiative transitions of the target atoms giving rise to a discrete spectrum.

The target is typically made of a metal of high atomic number, such as tungsten (W) or rhenium (Re) with thickness in the order of 0.1…1 mm depending on the rated voltage. Only a very small fraction of the electron beam energy is actually converted to photon energy emission rendering the X-ray generation inefficient with typical efficiencies of order 0.1…1%. The remainder of the energy is absorbed by the target and the substrate material of the anode body used both as a heat sink and main mechanical component of the anode carrying the target material. In view of the high thermal load, typically refractory metal alloys on molybdenum (Mo) basis are employed for the anode body.

Anodes of low rated voltage can be designed as stationary, actively cooled devices (Figure 2, left). However, with increasing rated power, different design concepts must be employed to control the thermal loads and avoid damage. Though there exist other approaches such as the *metal jet anode* [2], most of these designs aim at effectively moving the focal spot over the target surface. This can be either established by a rotating anode (Figure 2, right) spinning at a constant rate ($10^3 \ldots 10^4$ rpm) with a spatially fixed eccentric electron beam (Figure 1) or by steering the electron beam emitted from a concentric cathode around the anode by electro-magnetic lenses in the framework of *rotating envelope tubes*.

Figure 2. Stationary X-ray anodes made of Cu (left) and rotating X-ray anode made of Mo-alloy with graphite body (right), all with WRe-alloy focal tracks (Plansee SE).

Though this allows to make use of a stationary anode with very efficient cooling, the entire tube assembly must be rotated to direct the emitted X-ray photons to the X-ray window of the housing.

In addition, area-specific thermal loads are commonly reduced making use of the *line focus principle* [3]: By inclining the target surface with respect to the axis of electrodes and electron beam by a few degrees and arranging the line of sight through the X-ray window (Figure 1, W) perpendicular to the latter, the electron beam can be stretched in the direction of inclination. This effectively increases the actual focal spot size of the incident electron beam determining the area of heat deposition and still ensures the desired small effective focal spot size for emitted X-ray photons.

Hence, efficiency and heat deposition of a solid X-ray anode for a given target material are mostly determined by target thickness, target inclination as well as shape and power of electron beam.

Modeling of radiation transport

Modeling of X-ray radiation transport by electrons and photons through matter can give valuable quantitative insight into the performance of a target and the emitted spectrum. Since continuum-based approaches based on the BOLTZMANN transport equations are usually limited to idealized geometrical configurations, particle-based approaches in the framework of the Monte Carlo method are well suited for this purpose [4]. They aim at resolving the cascade, or *shower*, of photons and secondary electrons from electrons impinging on the target and produced by interactions with target atoms. To this end, the history of a sufficiently large number of particles is tracked by random sequences of free flights with subsequent atomic interactions. The latter are characterized by a loss of energy, deflection and possibly secondary particle emission which are all determined by random sampling methods. Tracking is performed until particles are either lost from the computational domain or their energy has depleted such that they become absorbed by the solid material. Both mechanisms yield the required information about particle and energy fluence and energy deposition, respectively.

Atomic interaction model

The model considers all interactions [4] of electrons and photons with atoms of given atomic number Z relevant for the typical energy range found in X-ray applications [2]. Interaction data, in particular, cross sections are compiled for application-relevant atomic numbers $Z = 42$ (Mo), $Z = 74$ (W), and $Z = 75$ (Re) from the EPICS-database [5] published by the IAEA.

Electron interactions with atoms

Elastic scattering (Figure 3, left) of electrons is the most frequent interaction contributing to significant scattering of electrons. Due to the atom-to-electron mass ratio of $3600 \cdot Z \cdot m_e$ the energy transfer to the atom is negligible allowing to consider the interaction solely as the deflection of the imping electron. As a simplification, isotropic scattering is assumed.

Inelastic scattering (Figure 3, center) comprises electronic excitation and ionization leading both to the deflection of the imping electron and its energy loss W related to the binding energy of the ionized subshell U_i. In case of ionization events, a secondary electron is emitted, whereas electronically excited atoms subsequently relax to ground state contributing to characteristic X-ray emission.

Bremsstrahlung emission (Figure 3, right) is the main source for photon production yielding a continuous energy spectrum. High energy electrons become decelerated in the vicinity of atomic nuclei consequently experiencing an angular deflection and energy loss W corresponding to the initial energy of the emitted photon.

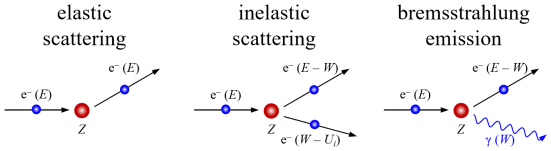

Figure 3. Atomic interactions of electrons [4].

Photon interactions with atoms

Photoelectric absorption (Figure 4, left) of photons, on the other hand, can be regarded as the main absorption mechanism of photons. Photons become absorbed by a subshell of an atom leading to emission of a secondary electron and leaving an electronically excited atom. The latter eventually relaxes to ground state again contributing to characteristic X-ray emission.

Incoherent or RAYLEIGH scattering (Figure 4, center) results from interaction of a photon with a *tightly* bound atomic electron. Being a type of elastic interaction it solely results in an angular deflection of the imping photon.

Interaction of photons with *loosely* bound atomic electrons leads to coherent or COMPTON scattering

(Figure 4, right). The impinging photon becomes absorbed emitting both a secondary photon of lower energy $E' < E$ and an electron of energy $E - E' - U_i$ as well as leaving an excited atom with a vacancy in subshell i of binding energy U_i, subsequently relaxing to ground state by radiative transitions. For implementation convenience, absorption of the primary and emission of the secondary photon is considered by scattering and energy loss of the imping photon.

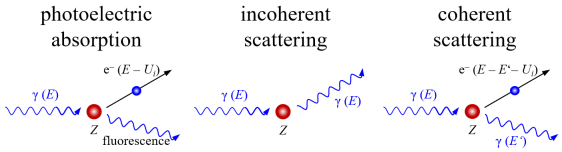

Figure 4. Atomic interactions of photons [4].

Implementation in COMSOL Multiphysics

The model is implemented in COMSOL Multiphysics 6.1 using the *Particle Tracing Module*. Since there is currently no dedicated physics interface or feature for coupled electron-photon transport available, a great deal of customization is required to achieve this goal. To this end, either the *Mathematical* or *Charged Particle Tracing* interface can serve as the basis for implementation offering the same set of required features. Since the latter, however, offers some features potentially useful for electron transport, this seems the more natural choice though the underlying physics are not specifically considered to be related to charged particles.

Particle types

The model accounts for three different particle types or species: In a first place it considers the primary electrons (e^-) incident to the target. Since the electron trajectories from the cathode to the anode are not relevant for the modeling scope and on the other hand an ideal monoenergetic pencil beam can be assumed [2], electrons are released at the point of incidence on the target with identical initial kinetic energy defined by the cathodic bias. To this end, electrons are released at discrete time instants using the *Release from Grid* feature. During their trajectories through the solid target medium, the electrons occasionally emit photons through Bremsstrahlung emission.

Photons (γ) are thus considered as the second particle type. Both electrons and photons contribute to the population of electrons by secondary electron emission occurring during inelastic scattering and photo-electric absorption as well as incoherent scattering, respectively.

The same interactions also leave the neutral atom in an electronically excited state. Excited atoms A^* will eventually relax to their ground state contributing to the energy deposition within the solid medium. Thus, excited atoms are considered as a third species. They will not perform any trajectories and are currently only used to consistently account for energy transfer to the solid medium and to perform energy and particle statistics. Considering them as a separate species, however, would allow to account for their relaxation to ground state through a series of radiative and non-radiative transitions in a more detailed fashion.

The three different particle types implemented by the *Particle Properties* feature essentially only serve as labels making the selection of applicability of subsequent features such as secondary emission and accumulators more convenient. Other than that, the particles behave the same.

Particle trajectory integration

Since the Monte Carlo model of radiation transport is based on the idealization of each electron and photon trajectory as a series of free flights followed by an atomic interaction, these can be integrated along their path length with the length of the free flights sampled from the respective probability density function (PDF) [4] and the total mean free path length. Hence, the model does not exhibit an intrinsic physical time but rather uses a pseudo-time allowing for integration using the *Time Dependent* study step. As a convenient choice, the pseudo-time scale is chosen such that unit time corresponds to a single free flight step. Consequently, the equations of motion underlying the particle tracing interface can be replaced by a series of free flights described by the particle positions at the end of each. This implies that the mass of the particle (zero for photons) does not enter the set of equations for integration of particle paths. Since the *massless* formulation available with the *Mathematical* and *Charged Particle Tracing* interfaces does not support the *Velocity Reinitialization* features required for description of atomic interactions, one has to resort to the standard NEWTONIAN formulation solving for the spatial position vector $\mathbf{q}$ of the particles. Hence, all particles are assigned a fictitious (unit) mass and the particle velocity reduces to a pseudo-velocity to be determined in consistent fashion from the pseudo-time and the path length.

Particle variables

This in turn implies that the particle (kinetic) energy (built-in variable *pt.Ep*) cannot be computed from the particle mass and velocity anymore. Consequently, it must be considered by a separate scalar state variable implemented as an *Auxiliary Dependent Variable*.

An additional auxiliary dependent or state variable is required to describe the shower number n_s of each particle which equals the number of the initial primary electron incident to the target. This allows to trace back all secondary particles to their origin and to perform the required statistics over all

showers. For statistical and detailed analysis purposes, additional optional state variables account for the number and type of collisions for each particle.

Atomic interactions
All atomic interactions of electrons and photons are considered using the *Velocity Reinitialization* feature. The reinitialization condition considers the particle type and the relative probability of a certain atomic interaction deciding which of the relevant interactions applies. If the condition is met, the pseudo-velocity vector and all state variables are reinitialized depending on the type of interaction. The pseudo-velocity vector is computed from the length of the next free flight and the scattering direction decomposed into polar and azimuthal components. The azimuthal scattering angle φ is sampled from a uniform probability density function from the interval $(0, 2\pi)$ corresponding to the simplified assumption of isotropic scattering. The polar angle θ, on the other hand, is determined from the probability density function specific for the given atomic interaction. The same applies to the energy loss W potentially experienced by the imping particle.

With the particle energy updated, the length of the next free flight $s(E)$ can be sampled from the corresponding PDF using a uniformly distributed random number ξ and the total mean free path length $\lambda_T(E)$. Finally, the remaining state variables related to interaction statistics are updated. For those atomic interactions leading to the (potential) emission of secondary particles (electrons or photons) or electronic excitation of target atoms, *Secondary Emission* features are used to initialize the pseudo-velocity vector, initial energy and the remaining state variables. The initial pseudo-velocity vector is again characterized by the initial total free path length and the polar and azimuthal angles with respect to the direction of the primary particle prior to the interaction. All quantities are sampled from probability density functions appropriate for the atomic interaction.

Particle and energy absorption
Over the series of atomic interactions that the primary particles experience, they continuously lose energy until depleted to a level not relevant for photon emission and transport. Hence, particles found within the computational domain whose energy becomes smaller than a certain cutoff (e.g. 10 eV) are discarded from the analysis after their energy is deposited at their current position. This is implemented using an additional *Velocity Reinitialization* feature, which effectively lets the particle disappear, whereas energy deposition is accounted for by a domain-based *Accumulator* feature.

From the obtained energy deposition field $w(\mathbf{x})$ in dimensions of energy per volume, one can compute the more commonly used absorbed dose distribution $D(\mathbf{x}) = w(\mathbf{x})/\rho$ in dimensions of energy per mass (SI-units: Gy = J/kg) using the density ρ of the solid material.

Additional optional domain-based accumulators are used to integrate the absorption of particles per type to perform particle balance checks for validation purposes.

Wall conditions
On the other hand, particles might leave the computational domain by successive scattering before experiencing sufficient energy loss. In this context, two cases are distinguished:

First, particles might leave the computational domain via the target surface. In case of electrons, it is assumed that the small fraction of ejected electrons is effectively rejected by the electric field and again impinges the target along the primary electron beam direction. This is accomplished by means of a *Wall* feature of general reflection type. Photons passing through the target surface on the other hand determine the X-ray photonic emission and are thus of primary interest. Using boundary-based accumulators, both photons and their energies are registered giving rise to the dosimetry quantities of photon fluence $\Phi_\gamma(\mathbf{x})$ (in dimensions of number per area) and photon energy fluence $\Psi_\gamma(\mathbf{x})$ (in dimensions of energy per area), respectively. Once registered, photons passing through the target surface are discarded from the simulation by using an appropriate wall condition. Photons pass through the target surface in arbitrary directions with only a small fraction of them directed towards the X-ray window and able to escape the X-ray tube housing. Consequently, an additional set of fluence fields $\Phi_{\gamma,\mathrm{det}}(\mathbf{x})$ and $\Psi_{\gamma,\mathrm{det}}(\mathbf{x})$ is computed considering only those photons that will leave the target surface in a direction allowing registration by the detector. Furthermore, the photons leaving the target can be classified according to their energy level and counted in histogram fashion yielding the photon energy spectrum as the (relative) number of photons of energy within a certain interval.

As a second case, particles might also pass through the boundaries of the segment of the physical domain used as computational domain. In the latter case, both electrons and photons are registered in terms of particle numbers and energies yielding electronic and photonic particle fluences $\Phi_{e/\gamma}$ and energy fluences $\Psi_{e/\gamma}$, respectively. Particles of sufficient energy level leaving the segment of physical domain chosen as computational domain through a solid boundary might re-enter the segment subsequently and contribute to the results in the

computational domain. Hence, the size of the computational domain must be chosen sufficiently large to minimize the portion of particles leaving through solid boundaries. Hence, fluences over solid boundaries serve as a means to verify a reasonable choice for the size of computational domain.

General aspects for accumulators
All domain and boundary-based accumulators are formulated as density-quantities and solved on a sufficiently fine regular grid. Since deposition and fluences become less important with increasing depth from the target surface, the grid can be coarsened along this direction reducing computational costs.

The volume and surface field dosimetry quantities of absorbed dose $D(\mathbf{x})$, fluence $\Phi_{e/\gamma}(\mathbf{x})$ and energy fluence $\Psi_{e/\gamma}(\mathbf{x})$, respectively, are obtained in cumulative fashion for the number of particles representing incident electrons. In order to calculate objective dosimetry quantities, these are normalized by the number of incident electrons N_e as $\overline{D}(\mathbf{x}) = D(\mathbf{x})/N_e$, $\overline{\Phi}(\mathbf{x}) = \Phi(\mathbf{x})/N_e$, $\overline{\Psi}(\mathbf{x}) = \Psi(\mathbf{x})/N_e$, respectively. Furthermore, they can be rephrased as rate quantities per unit current by dividing them by the unit charge e.

Sampling algorithms
One of the fundamental aspects of the model is the physically sound resolution of atomic interactions. Hence, a great deal of work is devoted to the correct and yet efficient implementation of sampling algorithms and generation of random numbers. The basis for all sampling algorithms forms a random-number generator sampling random numbers ξ uniformly distributed in the interval (0, 1) taking a sufficiently large number of arguments to avoid formation of patterns. In the present, the pseudo-time step number n_t, the particle energy E, one interaction-specific index, and one particle-related index are employed. For the latter, it is distinguished between random numbers that need to be independent for primary and secondary particles and those that must be reproducible during secondary particle emission from the random numbers sampled for the primary particles. This is particularly important to ensure energy conservation when sampling the initial energy of secondary particles consistent to the energy loss of the primary ones. Whereas the particle-number n_p is used for intrinsically independent random numbers, the shower-number n_s is passed to the generator for reproducible random numbers.

Probability density functions (PDF) given in analytical fashion whose cumulative PDF can be inverted in closed form such as the exponential distribution of the free path length $p(s)$ [4], can be sampled using the inverse transform method in straightforward fashion. The same approach can also be applied to discrete distributions such as the one for the probabilities of atomic interactions of a particle with given energy.

Continuous distributions given in numerical fashion and locally exhibiting large gradients such as the momentum transfer magnitude q relevant for coherent scattering of photons require advanced sampling techniques such as the *rational inverse transform with aliasing* (RITA) method [4]. It combines sampling for a discrete distribution and rational interpolation on a (non-uniform) grid adaptively determined beforehand and providing the required interpolation error.

Another class of random sampling technique is the *rejection method* [4]applicable to distributions whose cumulative PDF cannot be inverted in closed form. To this end, the original PDF is multiplicatively decomposed using a candidate function of known inverse transform. Inserting the value sampled from the candidate function into the original PDF is used to decide if the value is accepted or rejected. In the latter case sampling is repeated rendering the method iterative.

The sampling algorithms are implemented in the framework of an extensive library of functions comprising both native analytical and external functions implemented in C++ and provided as a DLL. The latter approach is especially useful for iterative methods, since analytical functions do not support recursive calls.

Integration scheme
Particle population size is governed by shower evolution requiring allocation of numerous secondary particles making integration computationally expensive even for a moderate number of incident electrons and when resorting to the COMSOL option to *reuse disappeared particles*.

Due to their mutual independence, however, each shower can be treated individually. Hence, any combination of parallel and sequential runs can be performed to establish statistically representative results. Results from consecutive runs can simply be superimposed in terms of field dosimetry quantities and spectra to obtain the full set of results.

Convolution of results for pencil beam
The implementation of the transport model given above is formulated for an ideal monoenergetic electron pencil beam [2] for the given tube potential and electron kinetic energy, respectively. Assuming an isotropic solid medium, the obtained results can be transformed to an arbitrarily shaped finite electron beam profile using the convolution theorem [2] with the electron beam profile serving as kernel function. This can be performed in an inexpensive postprocessing computation or separate stationary study step.

Application

Exemplary application is shown for a pure tungsten (W, $Z = 74$) target of 0.85 mm thickness bonded onto a pure molybdenum (Mo, $Z = 42$) substrate and inclined at 10° with respect to the anode and electron beam axis, respectively. The computational domain is chosen as a cube of 1.5 mm side length as shown in Figure 5. The detector is assumed as a circular area found at a distance of 10 mm from the focal spot with its center found on the line normal to the anode axis and an angle of aperture of 45°. The cell size used for the accumulators is 20.0 µm in the target surface plane and 50.0 µm in thickness direction. The focal spot is chosen as the origin of the global coordinate system with the z-axis aligned to the electron beam axis. For representation of fluence results a local coordinate system with the $\xi\eta$-plane aligned to the target surface is employed (see Figure 5). A moderate tube potential of 50 kV is assumed for the electron beam sampled by $N_e = 3 \cdot 10^5$ primary electrons and showers.

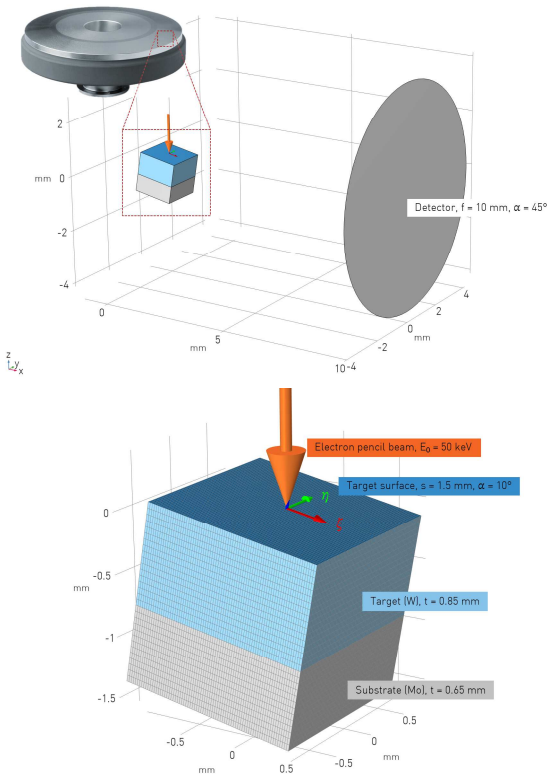

Figure 5. Schematic of target segment from a typical rotating X-ray anode and detector (top), computational domain with accumulator grid (bottom).

The results obtained for the electron pencil beam are given in Figure 6 in terms of target photon fluence $\bar{\Phi}_\gamma(\xi, \eta)$ and energy fluence $\bar{\Psi}_\gamma(\xi, \eta)$ per incident electron in logarithmic scales. Expectedly, the maximum fluences are found at the focal spot and the distributions appear symmetric with respect to the axis $\eta = 0$. In contrast, the distributions show a slight bias towards $\xi > 0$ which is attributed to the inclination of the target increasing the probability of photons to escape the target from shallower zones. As seen from the distributions, the main emission is found within a circle of app. 1 mm in diameter for the pencil beam at the given tube potential.

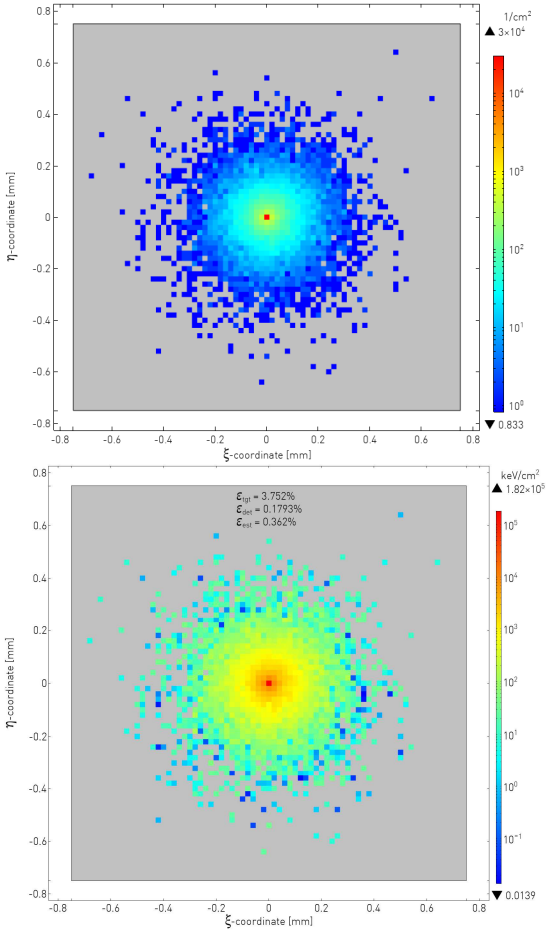

Figure 6. Photon fluence $\bar{\Phi}_\gamma(\xi, \eta)$ (top) and photon energy fluence $\bar{\Psi}_\gamma(\xi, \eta)$ (bottom) per incident electron with efficiency factors (insert) for electron pencil beam.

The total photon energy emitted by the target surface is found to be app. 3.75% of the incident electron energy. Filtering photon fluence using the given detector plane reveals that only app. 5% of the emitted photon energy represents utilizable X-radiation reducing the overall efficiency to app. 0.18%. These results are plausible from their order of magnitude both from practical experience and when compared to estimates based on the atomic number Z and the incident electron energy E_0 [3], [6] obtained as app. 0.36%.

The absorbed dose distribution $\bar{D}(\mathbf{x})$ per incident electron of the ideal electron beam is depicted in Figure 7 in logarithmic scale by means of contours over the section planes $\xi = 0$ and $\eta = 0$, respectively together with iso-surfaces separated by orders of magnitude. The distributions confirm the observations already made for the target fluences with respect to symmetry about the plane $\eta = 0$. Furthermore, again a slight bias towards $\xi > 0$ is observed

aligned to the direction of the pencil beam. Almost the entire energy is dissipated within the target material, thus, not directly affecting the substrate for the given tube potential. It is, however, expected that the effective “penetration depth” of the beam will increase with higher tube potential.

Furthermore, Figure 7 depicts exemplary tracks of electrons (orange) and photons (blue) for ten randomly selected showers. In addition, arrows indicate the direction of emission for a sample of emitted photons colored by their radiant energy *k*.

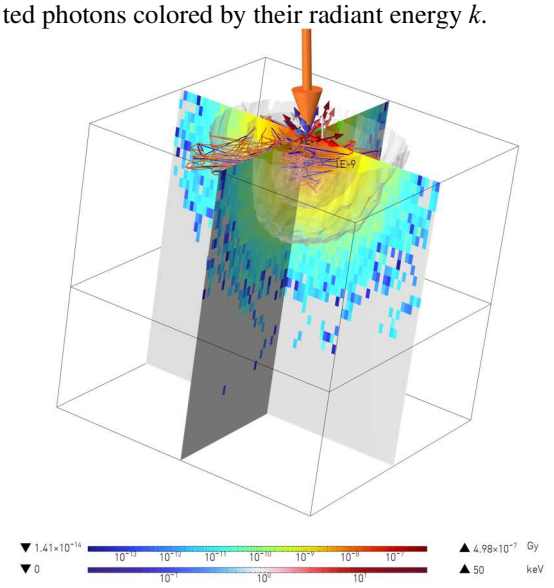

Figure 7. Absorbed dose distribution $\overline{D}(\mathbf{x})$ per incident electron (contours, iso-surfaces) for electron pencil beam with exemplary electron (orange) and photon (blue) tracks for 10 showers with photon emission (arrows colored by radiant energy k).

Outlook

The model successfully implemented in COMSOL Multiphysics will be further enhanced with respect to more detailed resolution of elastic and inelastic scattering events of electrons in the future. Further development will also focus on performance improvements allowing to resolve an increased size of particle population in efficient manner.

From the application point of view, the model will be applied to parametric assessments of solid X-ray target configurations as the one shown in the present paper to study the influence of main design parameters such as tube potential, target thickness and angle on dosimetry quantities.

Finally, the absorbed dose distributions obtained with the model will help to strengthen the understanding of heat source distributions used in nonlinear cyclic thermo-mechanical finite element analyses routinely performed in the process of design and strength assessments of stationary and rotating X-ray anodes.

References

[1] wikipedia:User:ChumpusRex, "X ray tube in housing," https://commons.wikimedia.org/wiki/File:Xraytubeinhousing_commons.png, Accessed: 2024-08-28.

[2] G. Luani, "Optimization of e-beam and x-ray target," Master Thesis, University of Uppsala, 2021.

[3] G. Poludniowski, A. Omar and P. Andreo, Calculating X-ray Tube Spectra - Analytical and Monte Carlo Approaches, CRC Press Taylor & Francis Group, 2022.

[4] F. Salvat, "PENELOPE-2018: A Code System for Monte Carlo Simulation of Electron and Photon Transport," Workshop Proc., Barcelona, Spain, 2019.

[5] D. E. Cullen , "EPICS2017 – Electron Photon Interaction Cross Sections," International Atomic Energy Agency (IAEA), Vienna, Austria, 2017.

[6] H. W. Koch and J. W. Motz, "Bremsstrahlung cross-section formulas and related data," *Rev. Mod. Phys. (31),* pp. 920-955, October 1959.